Site-Directed Spin-Labeling of Transmembrane Domain VII and the 4B1 Antibody Epitope in the Lactose Permease of *Escherichia coli*†

John Voss,‡ Wayne L. Hubbell,§ Jordi Hernandez-Borrell,‡,|| and H. Ronald Kaback*,‡

Howard Hughes Medical Institute, Departments of Physiology and Microbiology & Molecular Genetics, and Jules Stein Eye Institute and Department of Chemistry & Biochemistry, University of California, Los Angeles, California 90095-1662

Received July 15, 1997; Revised Manuscript Received September 25, 1997⊗

ABSTRACT: Functional lactose permease mutants containing single Cys residues at positions 233−255 and a biotin acceptor domain at the C terminus were solubilized in dodecyl β-D-maltopyranoside and purified by avidin affinity chromatography. Each mutant protein was derivatized with a thiol-selective nitroxide reagent and examined by conventional and power saturation electron paramagnetic resonance spectroscopy (EPR). The EPR spectral line shapes and the influence of nonpolar O_2 or polar potassium chromium oxalate relaxation agents on the saturation behavior of the spin-labeled proteins were measured in order to obtain information on the mobility of the spin-labeled side chains and their accessibility to the relaxation agents, respectively. The results provide evidence that residues Ser233−Asn246 are within the hydrophobic core of the membrane and that Phe247 is at the lipid headgroup−solvent interface. Along with Phe247, Phe250 and Gly254 are also surface-exposed, as indicated by studies on the epitope for monoclonal antibody 4B1 [Sun, J., Wu, J., Carasco, N., and Kaback, H. R. (1996) *Biochemistry 35*, 990−998]. Furthermore, the nitroxide-labeled intramembrane Cys replacements exhibit variations in mobility and accessibility that are consistent with the conclusion that TM VII is an α-helix in contact with surrounding helices in the tertiary structure of the permease.

The lactose permease (lac permease)[1] of *Escherichia coli* is a polytopic membrane transport protein encoded by the *lacY* gene. The permease has been solubilized from the membrane, purified, reconstituted into proteoliposomes, and shown to be solely responsible for the coupled stoichiometric translocation of β-galactosides and H^+ as a monomer (reviewed in ref 1). All available experimental evidence indicates that the permease is composed of 12 α-helical rods that traverse the membrane with the N and C termini in the cytosolic side (Figure 1). Moreover, application of a variety of site-directed biochemical and biophysical techniques, as well as identification of discontinuous monoclonal antibody epitopes, has led to a description of helix packing in the permease (reviewed in ref 2). The structural data in conjunction with extensive mutational analysis have led recently to a model that provides a mechanism for coupling between substrate and H^+ translocation in the permease (*3*).

Site-directed spin-labeling (SDSL) is a particularly valuable technique for investigating membrane protein structure and dynamics (reviewed in refs 4 and 5). The method involves introduction of a single Cys residue into a protein by site-directed mutagenesis, followed by labeling with a thiol-specific reagent containing a nitroxide spin-label. SDSL of proteins has been used to study secondary structure and/or dynamics (*4*, *6*), to measure distances between two paramagnetic centers (*7*−*12*), and to identify sites of tertiary interaction (*4*, *13*, *14*).

Cys-scanning mutagenesis of transmembrane domain VII (TM VII) and the periplasmic residues linking TMs VII and VIII (loop VII/VIII) in the permease (*15*) demonstrates that none of the residues are irreplaceable with respect to active transport. However, a number of observations indicate that this region is in an α-helical conformation and plays a role in the mechanism. (i) A sharp increase in alkaline phosphatase activity is observed as the fusion junction between the permease and alkaline phosphatase proceeds from Try228 to Ile230, suggesting that these residues approximate the middle of a transmembrane helix (*16*). (ii) TM VII contains two structurally important residues, Asp237 and Asp240, which are in close proximity to Lys358 (TM XI) and Lys319 (TM X), respectively (*15*, *17*−*22*). (iii) TM VII is close to the sugar translocation pathway, as demonstrated by site-directed chemical cleavage (*23*), chemical cross-linking, and spin-label dipolar interaction studies (*12*). (iv) Several single-Cys mutants in this region are inactivated by *N*-ethylmaleimide (NEM) (*15*), and these positions cluster on a face of TM VII that is oriented toward a common interface formed by TMs VIII, IX, and X which contain the irreplaceable residues Glu269, Arg302, and His322/Glu325, respectively. Moreover, Frillingos et al. (*24*) found that at least two Cys replacement mutants at positions within this domain

† The research reported here was supported in part by NIH Grant DK51131 to H.R.K. and NIH Grant EY05216 and the Jules Stein Professorship Endowment to W.L.H. J.H. was supported by a fellowship from the Gaspar de Portola Catalonian Studies Program.

* To whom correspondence and reprint requests should be addressed.

‡ Departments of Physiology and Microbiology & Molecular Genetics.

§ Jules Stein Eye Institute and Department of Chemistry & Biochemistry.

|| Present address: Department of Physical Chemistry, Facultat de Farmacia, UB, 08028 Barcelona, Spain.

⊗ Abstract published in *Advance ACS Abstracts,* November 1, 1997.

[1] Abbreviations: SDSL, site-directed spin-labeling; methanethiosulfonate spin-label, (1-oxyl-2,2,5,5-tetramethylpyrroline-3-methyl)-methanethiosulfonate; EPR, electron paramagnetic resonance; TM, transmembrane domain; loop VII/VIII, periplasmic loop between TMs VII and VIII; lac permease, lactose permease; mAb, monoclonal antibody; DPPH, 2,2-diphenyl-1-picrylhydrazyl; KP_i, potassium phosphate; SDS, sodium dodecyl sulfate; PCR, polymerase chain reaction; DM, *n*-dodecyl β-D-maltopyranoside; CrOx, potassium chromium oxalate (potassium trioxalatochromate).

S0006-2960(97)01726-1 CCC: $14.00

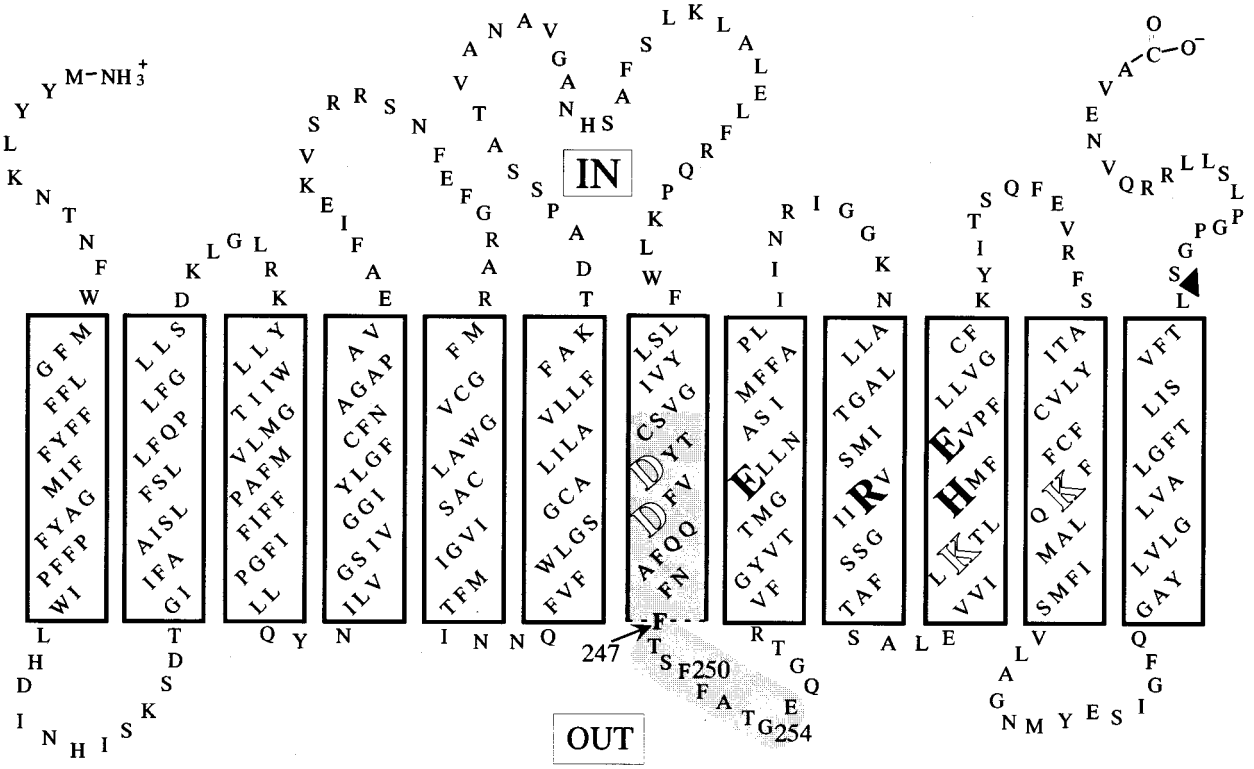

FIGURE 1: Secondary structure model of lac permease. The single-letter amino acid code is used; transmembrane α-helical domains are boxed, and the residues in domain VII and loop VII/VIII studied by SDSL are shaded gray. The solid arrowhead indicates the insertion point of the biotin acceptor domain. Enlarged, solid letters represent irreplaceable residues, and enlarged, empty letters represent charge pairs [Asp237 and Asp240 (TM VII) with Lys358 (TM XI) and Lys319 (TM X), respectively].

exhibit significantly altered reactivity with NEM in the presence of substrate. (v) The epitope for monoclonal antibody (mAb) 4B1 which uncouples lactose from H^+ translocation (*25*, *26*) is comprised of Phe247, Gly254, and Phe250 as determinants, in order of importance, and the three positions cluster on the same face when the region is modeled as a helical wheel (*27*, *28*). (vi) Site-directed thiol cross-linking of TMs VII and II inactivates the permease in a manner that is reversed by reducing agents, indicating that conformational flexibility between the two TMs is important for turnover (*29*).

In this paper, SDSL is used to study single-Cys replacement mutants in TM VII and loop VII−VIII which contains the 4B1 epitope (Figure 1). On the basis of the analysis of side chain mobility and accessibility to molecular O_2 and chromium oxalate, we conclude that TM VII is in an α-helical conformation surrounded by other transmembrane domains in the tertiary structure. Furthermore, evidence is presented demonstrating that the residues comprising the 4B1 epitope are solvent-exposed with Phe247, the primary determinant, at the phospholipid headgroup−solvent interface on the periplasmic side of the permease.

EXPERIMENTAL PROCEDURES

Materials

(1-Oxyl-2,2,5,5-tetramethylpyrroline-3-methyl)methanethiosulfonate (methanethiosulfonate spin-label) was a gift from K. Hideg and is available from Reanal (Budapest, Hungary). Deoxyoligonucleotides were synthesized on an Applied Biosystems 391 DNA synthesizer. All restriction endonucleases and T_4 DNA ligase were from New England Biolabs (Beverly, MA). Sequenase was from United States Biochemical (Cleveland, OH). All other materials were reagent grade and obtained from commercial sources.

Methods

Construction, Expression, and Purification of Mutant lac Permeases. Construction of the single-Cys mutants used in this study has been described (*15*). To facilitate avidin affinity purification, the gene encoding the biotin acceptor domain from a *Klebsiella pneumoniae* oxaloacetate decarboxylase was inserted at the C terminus (*30*) of mutants containing single Cys residues at positions 233−255 by restriction fragment replacement. SDSL studies on single-Cys mutants at positions 237 and 240 have been described (*16*) and were omitted from this study. After the desired mutations were confirmed with dideoxynucleotide sequence analysis, *E. coli* T184 (*lacZ*$^-$*Y*$^-$) was transformed with a plasmid encoding a given mutant. Cells were grown aerobically at 37 °C in Luria-Bertani broth with streptomycin (10 μg/mL) and ampicillin (100 μg/mL). Dense cultures were diluted 10-fold in a 12 L fermentor and grown for 2 h at 37 °C before induction with 1 mM isopropyl 1-thio-β-D-galactopyranoside. After growing for another 2 h at 37 °C, cells were harvested and disrupted by passage through a French pressure cell. A membrane fraction was isolated by centrifugation and extracted with 3% DM (w/v), and permease was purified by affinity chromatography on immobilized monomeric avidin as described (*12*). Each preparation yielded a single band on silver-stained SDS/12% polyacylamide gels. Purified mutant protein was then incubated with 100 μM methanethiosulfonate spin-label for 30 min at room temperature to generate the nitroxide side chain R1 (Figure 2), concentrated, and dialyzed using a Micro-ProDiCon membrane (Spectrum) (*10*).

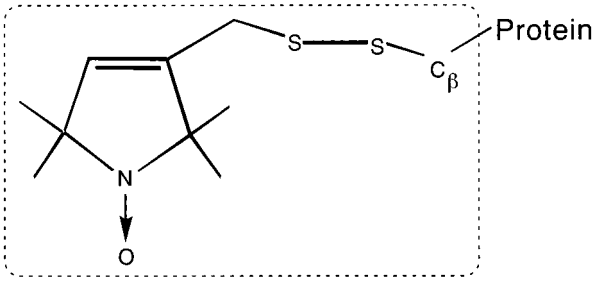

FIGURE 2: Structure of nitroxide side chain R1.

EPR Spectroscopy. EPR measurements were made on samples in TPX capillaries at 22 °C. Five to ten microliters of sample containing purified permease at a final concentration of ca. 50 μM in 10 mM MES (pH 7.5)/0.02% DM was used in each measurement. Spectra were obtained using a Varian E-109 X-band spectrometer fitted with a loop-gap resonator (*31*−*33*) at a microwave power of 2 mW and a modulation amplitude optimized to the natural line width of the individual spectrum and recorded under field-frequency lock at X-band. Signal-averaged spectra (four scans) were obtained with a 100 G sweep at 30 s/scan using a Nicolet 1280 computer.

Power saturation measurements were carried out as previously described (*34*) in a N_2 atmosphere, in the presence or absence of 20 mM CrOx or in the presence of O_2 in equilibrium with air. Data were analyzed in terms of the parameter $P_{1/2}$, which is proportional to $1/T_{1e}T_{2e}^2$ (*34*). $P_{1/2}$ is the microwave power which saturates the signal amplitude to $^1/_2$ the value it would have reached in the absence of saturation. Spin exchange with a fast-relaxing paramagnetic species such as O_2 results in an increase in the relaxation rate ($1/T_{1e}$) proportional to the collision frequency (*34*). The change in $P_{1/2}$ due to the presence of O_2, $\Delta P_{1/2} = P_{1/2}(O_2) - P_{1/2}(N_2)$, is a direct measure of the collision frequency of the nitroxide with O_2. To account for the effect of T_{2e} and variations in spectrometer performance, $\Delta P_{1/2}$ is normalized to give the "accessibility parameter", Π, defined as

$$\Pi = \frac{\Delta P_{1/2}}{P_{1/2}(\mathrm{DPPH})} \frac{\Delta H(\mathrm{DPPH})}{\Delta H}$$

where $P_{1/2}$(DPPH) is $P_{1/2}$ for a 2,2-diphenyl-1-picrylhydrazyl (DPPH) crystal, ΔH(DPPH) is the peak-to-peak line width of the DPPH resonance, and ΔH is the corresponding line width of the nitroxide central ($m_I = 0$) resonance (*35*).

RESULTS

Determination of the Periplasmic Surface Boundary of TM VII. EPR spectra of the R1 nitroxide side chain at positions 233−255 in transmembrane domain VII of lac permease are shown in Figure 3. The inverse of the line width of the central resonance, $1/\Delta H$, is an increasing function of the motional freedom[3] of the nitroxide in its local environment (*13*, *36*). A plot of $1/\Delta H$ *versus* the position of the R1 side chains in transmembrane domain VII reveals a fluctuation in the mobility of the residues that probably reflects tertiary

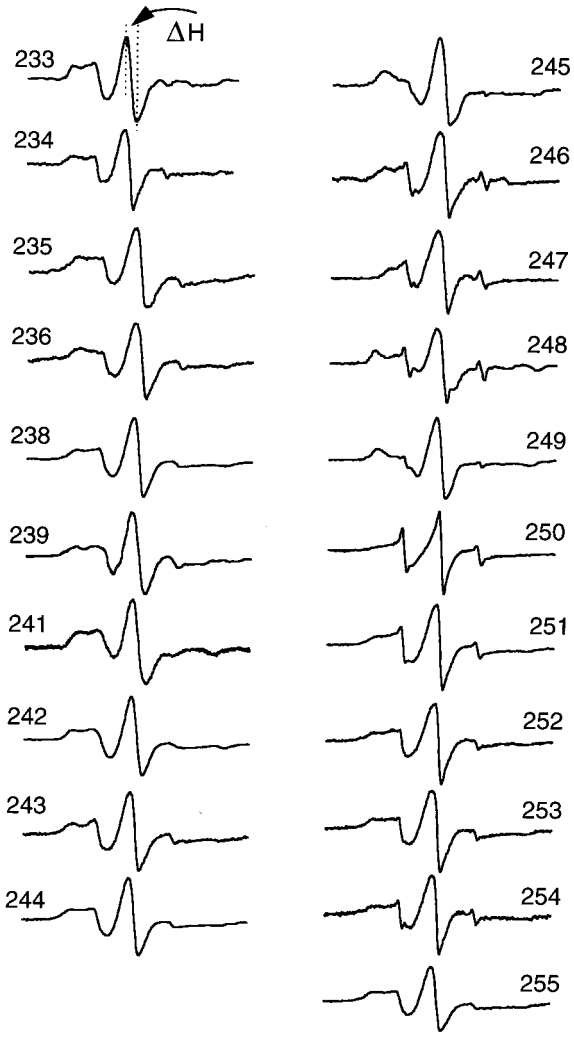

FIGURE 3: First-derivative EPR spectra of given nitroxide-labeled single-Cys mutants at positions 233−255, excluding positions 237 and 240 which were examined previously (*16*). The spectra are scaled vertically for convenience of presentation, and the magnetic field scan width is 98 G. The line width of the central resonance (ΔH) is indicated on the spectrum of residue 233.

contacts of the nitroxide side chains with other parts of the permease (*13*, *14*) (e.g. variations that arise from a helical structure in anisotropic interaction with the remainder of the protein; see Discussion). It is clear that nitroxides attached to positions at the C-terminal end (residues 249−255) of this sequence exhibit substantially higher motional freedom by this measure (Figure 4, open symbols), with position 250 displaying the most flexibility. The increased mobility displayed along the profile is consistent with the spin-label moving through an internal domain of the protein into a surface domain (*4*, *13*). In this domain (positions 247−255), there is a marked decrease in the mobility of positions 250−255, reflecting either a more stabilized backbone or greater steric interactions between side chains. It is also noteworthy that permease with a six-His insertion at position 255 is almost fully active (*37*), clearly indicating that the C-terminal end of the scanned region is outside of the membrane.

Another approach used in topological mapping is examination of the collision rate of R1 with diffusible paramagnetic species (*4*). $\Delta P_{1/2}$ is determined from the saturation behavior of the central resonance ($m_I = 0$) line in the absence and presence of a paramagnetic relaxing agent such as O_2. The accessibility parameter Π is derived from $\Delta P_{1/2}$ normalized

[2] T_{1e} is the spin lattice relaxation time; T_{2e} is the transverse relaxation time.

[3] The term motional freedom is used in a general sense, and a change in motional freedom can arise from a change in either the rate or amplitude of motion, or both.

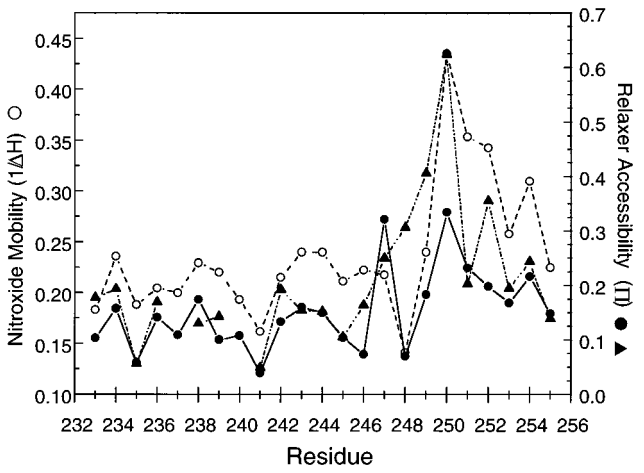

FIGURE 4: R1 side chain mobility and accessibility to O_2 or CrOx. $1/\Delta H$ (open circles), $\Pi(O_2)$ (filled circles), and Π(CrOx) (triangles) versus sequence position for the nitroxide-labeled single Cys residues at positions 233−255. The $\Pi(O_2)$ and $1/\Delta H$ data points for positions 237 and 240 are taken from ref 16. On the basis of the fit to $\Delta P_{1/2}$, the estimated error in Π values is less than ±10% SD. The estimated error in ΔH, based on spectral signal to noise, is no more than 5% for any given point.

to the intrinsic line width of R1 and the saturation behavior of a DPPH standard. Figure 4 (filled circles) shows $\Pi(O_2)$ as a function of R1 position in TM VII and loop VII−VIII. With the exception of position 247, the data display a profile virtually identical with that observed for nitroxide mobility (i.e. $1/\Delta H$) with the same periodicity.

More detailed topographical information can be obtained by examining the contrast individual sites display with respect to accessibility to a polar relaxation agent, such as CrOx, relative to molecular oxygen which is nonpolar. Thus, the saturation behavior of each mutant was measured in the presence of 20 mM CrOx. Since CrOx is preferentially localized in the aqueous phase, surface-exposed residues display a high collision frequency with this agent. Clearly, Π(CrOx) increases dramatically from F247 through F250 (Figure 4, closed triangles). Within the investigated region, the Π(CrOx) value at position 247 is 32% higher than that of any of the residues N-terminal to this position. The observation strongly suggests that F247 is the first residue in the region scanned that is accessible from the aqueous phase, a finding consistent with studies of Sun et al. (*27*) which identify Phe247 as the primary epitope determinant for mAb 4B1 (see below).

Analysis of Transmembrane Residues. The average mobility and accessibility of the transmembrane residues 233−246 (Figure 4) is lower than that observed for helix XII (*14*), thereby suggesting that TM VII is more sequestered. This observation is consistent with an experimentally derived packing model of the permease in which TM VII is surrounded by other helices (*38*), while most of the helix XII surface area is in contact with the hydrophobic phase of the membrane (*14*). Thus, the variation in the side chain dynamics and solvent accessibility (Figure 4) which correlate strongly is attributed to tertiary packing of this domain within the protein (see Discussion).

Analysis of the 4B1 Epitope. The 4B1 epitope is located in loop VII/VIII (Figure 1) (*27*). As a group, R1 side chains at the positions that comprise the epitope, 247, 250, and 254, have high mobilities and collision frequencies relative to those of the neighboring residues which is expected for sites accessible to an antibody. Consistent with the predicted hydrophilic environment for this region, several residues within the 247−255 sequence are surface accessible, as judged by side chain mobility in general and CrOx accessibility in particular. Compared to the transmembrane residues, the correlation between the accessibility parameters and side chain mobility is weaker. Of special interest is position 248 which exhibits a high collision frequency with CrOx but displays the lowest mobility of all the side chains examined in the study. Because of the high accessibility of position 248 to CrOx, dynamics at this position may not be restricted by tertiary contact, but by a turn in the backbone. This feature (high CrOx accessibility and low side chain mobility) is also demonstrated by two loop positions in bacteriorhodopsin: 103 (*39*) and 131 (*40*).

DISCUSSION

Analysis of the Transmembrane Residues. As demonstrated previously using spectral second moments and the inverse of the center spectral line (*4*, *13*, *14*), the mobility of nitroxide side chains may exhibit a periodicity indicative of a specific secondary structure. For example, a transmembrane α-helix may have one face on which the residues are relatively immobile due to contacts with other portions of the protein, whereas the residues occupying the remaining surface are more mobile because they are exposed to the lipid hydrocarbon chains. In this ideal case, a periodicity in the mobility parameter of approximately 3.6 is expected. In contrast, with a β-sheet structure under the same conditions, a periodicity of 2 is expected. In this study, a permease sequence was investigated that is predicted to pass through the hydrophobic bilayer into the periplasm. On the basis of the activity of serial alkaline phosphatase fusions (*16*) and on the basis of studies that probe the orientation of selected side chains with respect to sequence position (*12*), an α-helical secondary structure for TM VII is highly likely. Therefore, any periodicity due to anisotropic environments along the helix should be related to the predicted helix-packing arrangement for the permease.

The dynamics reported by an attached nitroxide may include contributions from rotational diffusion of the whole protein, motion of the side chain relative to the backbone, and motion of the backbone relative to the average structure. Since rotational diffusion of the permease in a DM micelle is too slow to effect the conventional EPR line shape, motional narrowing arises from the latter two types of motion. However, in a region of continuous secondary structure, the variability in backbone dynamics will be relatively small from one residue to the next, while the variability in side chain dynamics may be dramatic due to interactions with the surrounding milieu (*13*). On the basis of the outer splittings, which resolve individual dynamic components and the amplitude of each component, most of the spectra appear to be heterogeneous. In heterogeneous spectra, the center line width is dominated by the motion of the most mobile component. Thus, a spin-labeled side chain that samples two environments, partially buried or solvent-exposed, is classified as surface accessible according to $1/\Delta H$ analysis. Therefore, the $1/\Delta H$ parameter is useful in delineating residues which lack a highly mobile population.

Variations in $1/\Delta H$ attributed to periodic changes in tertiary contacts should be mimicked by the collision

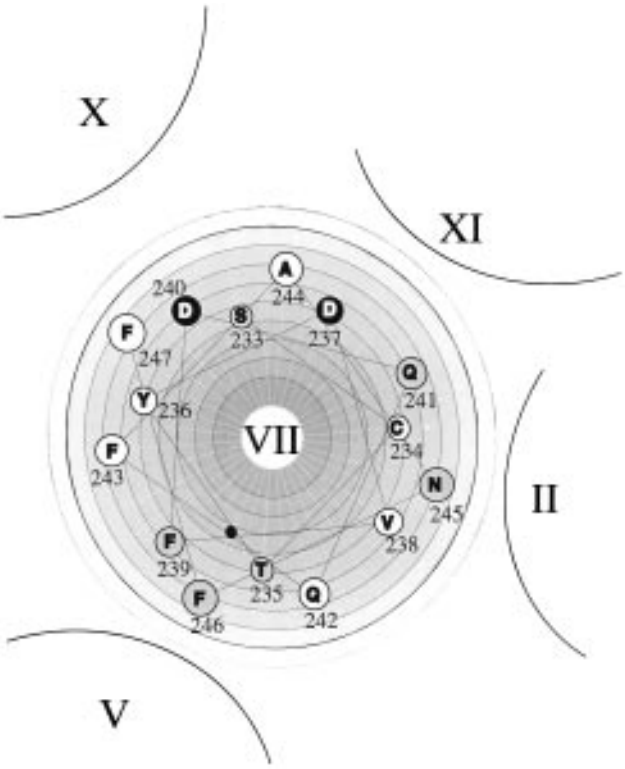

FIGURE 5: Helical wheel representation of the transmembrane portion of domain VII in lac permease. Numbered residues were investigated by SDSL. Positions which exhibit $\Pi(O_2)$ values of 0.1 or less (see the text) are highlighted in gray. The two Asp residues involved in charge pairs (black) were studied previously (*16*). The locations of neighboring helices relative to helix VII are indicated by the black semicircles. The solid black circle illustrates the position of Tyr228, which cross-links to helix V (*12*).

frequency (Π) of a small paramagnetic relaxer, such as O_2. The data presented in Figure 4 clearly reveal a pattern of changes in $\Pi(O_2)$ that are in phase with those of $1/\Delta H$, although the relative amplitudes of the oscillations in $\Pi(O_2)$ are different. As defined, "accessibility" of a nitroxide to O_2 is a function of both local steric constraints imposed by the protein structure and the product of the local diffusion constant and concentration, $D[O_2]$ (*34*). $D[O_2]$ in the micellar interior cannot be predicted, and variations in this parameter may contribute to variations in the amplitude of the maxima in $\Pi(O_2)$. However, by evaluating $\Pi(O_2)$ from a region scanned over several residues in conjuction with $1/\Delta H$ data, the precise value of $\Pi(O_2)$ is less critical, and more weight is given to the trend of the parameter.

By utilizing a variety of approaches, a packing scheme incorporating most of the transmembrane helices of lac permease has been proposed (reviewed in ref 2). The positions of helices X and XI relative to helix VII have been discussed extensively (*1*). Placement of these helices is based on charge pairing between Asp237 and Asp240 in helix VII with Lys358 (helix XI) and Lys319 (helix X), respectively, although the 240−319 interaction appears to occur over a longer range (*22*). In this packing arrangement, sites of tertiary contact that should display low collision frequencies with oxygen are predicted. The helical wheel diagram shown in Figure 5 illustrates the profile of $\Pi(O_2)$ in relation to the predicted packing scheme of the transmembrane domains in the permease with positions exhibiting $\Pi(O_2)$ values of 0.1 or less shown in gray. The proximity of helix VII to helix V (*12*) results in low oxygen accessibility at positions 239, 235, and 246. Likewise, low oxygen accessibility at positions 241 and 245 can be attributed to tertiary contacts with helix II which has also been shown experimentally to lie close to helix VII (*29*, *38*).

Interestingly, position 234 which is on the same face as position 245 exhibits higher accessibility to oxygen, while position 233 has lower accessibility than position 244. Possibly, the differences reflect tilting of helix VII so that the periplasmic (C-terminal) end of helix VII tilts toward helix II with the cytoplasmic end toward helix X. In the presence of substrate, the *N*-ethylmaleimide reactivity of V238C[4] permease is substantially reduced (*24*), and the EPR spectrum of V238R1 is broadened (not shown), suggesting increased tertiary contact at this site upon ligand binding. This change in reactivity following substrate binding may also involve movement of the periplasmic end of this domain (N245C) away from helix II (I52C and S53C) (*29*). Such a scissors-type movement may explain why position 238 which lies two turns above 245 comes into closer contact with the neighboring transmembrane domain.

Analysis of the Solvent-Exposed Residues. In addition to mapping the steric environment along a nitroxide-scanned sequence, elucidation of membrane protein topology also requires details on the location of residues relative to the membrane bilayer. The predicted topology of TM VII was initially modeled according to hydropathy analysis (*41*) and later revised to account for the charge pair between Asp237 and Asp240 (*17*). Subsequent analysis (*16*, *42*) of the topology of TM VII confirmed the placement of Asp237 and Asp240 within the membrane, but uncertainly remained with regard to the precise location of the periplasmic boundary of the domain. Characterization of the epitope for mAb 4B1 (*27*) demonstrates that Phe247 in periplasmic loop VII/VIII is the primary epitope determinant, indicating that this residue must be at or near the membrane−solvent interface. This conclusion is also supported by the functional complementation studies of Zen et al. (*42*) with contiguous, nonoverlapping permease fragments.

Nitroxide scanning of a membrane-spanning domain can be used to accurately delineate bilayer boundaries (*4*, *5*). As demonstrated with bacteriorhodopsin (*40*), as well as with visual rhodopsin (*43*), residues exposed to the aqueous solvent exhibit a high collision frequency with a polar relaxing agent, such as CrOx. In both proteins, sites with Π(CrOx) values of greater than 0.2 are assigned to hydrophilic surfaces. The findings are consistent with the known structural features of these proteins and, in addition, provide structural and dynamic information on the hydrophilic domains which is difficult to obtain by other means. Data presented in this paper demonstrate that there is a clear increase in Π(CrOx) at position 247 compared to that of the preceding residues (Figure 4, triangles). On the basis of Π(CrOx) values of 0.20 or greater for F247R1 and the succeeding positions, we conclude that this Phe247 is at the solvent−lipid headgroup interface with the succeeding residues outside of the membrane in the periplasmic loop VII/VIII.

[4] Site-directed mutants are designated by the single-letter amino acid abbreviation for the targeted residue, followed by the sequence position of the residue in the wild type lac permease and a second letter indicating the amino acid replacement.

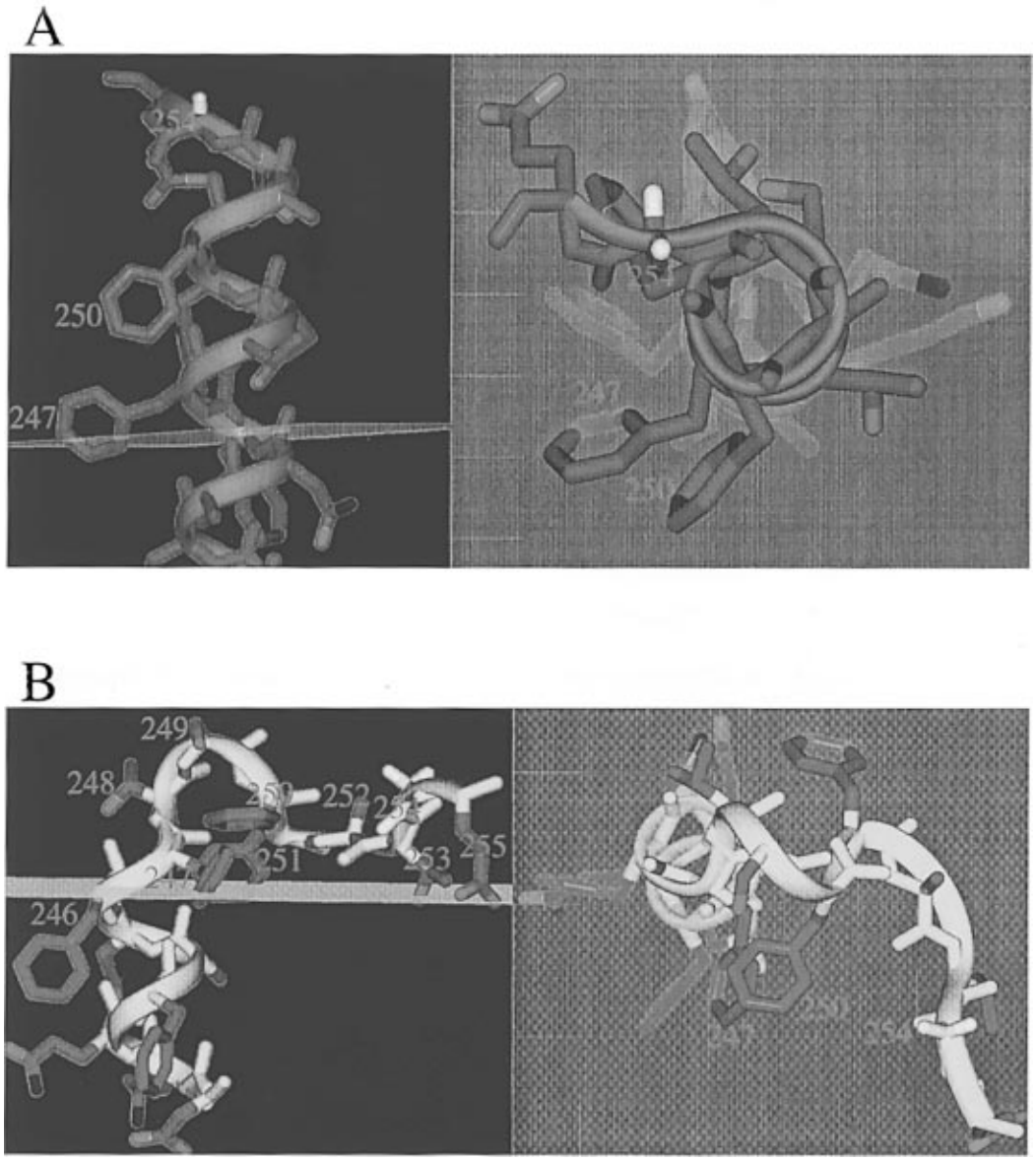

FIGURE 6: Molecular models of the C-terminal end of transmembrane domain VII and loop VII/VIII. The gray plane approximates the bilayer headgroup region. (A) α-Helical structure extends out of the bilayer with the 4B1 epitope residues numbered. (B) α-Helix with an inverse γ-turn about residues 246−248, followed by β-sheet structure involving residues 250−255. Modeling was performed using Insight II software (BIOSYM/Molecular Simulations).

By utilizing the known epitope determinants comprising the 4B1 epitope (*27*) in conjunction with the data obtained regarding the steric and polar environment of the positions within the epitope, the topography of the domain can be modeled. One possibility (Figure 6) is that the backbone retains α-helical structure as it extends out from the bilayer and terminates with a turn at position G254 (Figure 6A, left panel), an assumption consistent with the finding that permease with G254P binds 4B1 (*28*). An α-helical structure for the domain is consistent with the observation that the three residues that comprise the epitope (Phe247, Phe250, and Gly254) fall on one face of an α-helix (Figure 6A, right panel). In support of this, each of the three positions displays relatively high mobility and accessibility to relaxing agents (Figure 4). Furthermore, alkylation of single-Cys mutants at positions 252 and 253 by *N*-ethylmaleimide increases 4B1 binding (*27*). Such an effect suggests the side chains at these positions are similarly oriented, a geometry consistent with α-helical structure where positions 252 and 253 lie on the face opposite to the epitope determinants. In considering the model, the variability in the mobility and accessibility parameters for residues 247−255 is attributed to tertiary interactions with other parts of the protein, a contention supported by cross-linking of G254C with residues predicted to lie in the first periplasmic loop (*44*).

A second possibility is that there is a turn at positions 246−248, followed by a stretch of β-like secondary structure (Figure 6B). This model reflects both a plausible presentation of 4B1 epitope sites and a simple explanation for the collision frequency with the hydrophilic relaxer CrOx. Values of Π(CrOx) vary in amplitude from F250R1 through E255R1 with a periodicity of 2 (Figure 4). A plausible explanation for the profile is a β-like structure running parallel to the membrane surface (Figure 6B, left panel). Another attractive aspect of this model is the location of the turn. Turns are known to be highly antigenic (*45*), and in this model, the three epitope sites are brought close together via a turn (Figure 6B, right panel). Although Glu255 is oriented toward the lipid headgroups, it is possible that the carboxylate is H-bonded to the headgroup of phosphatidyl-

ethanolamine. Of the residues in the hydrophilic domain studied here, E255R1 displays the lowest CrOx accessibility and mobility (Figure 4), and Sun et al. (*27*, *28*) have proposed a turn at Gly254. Thus, the E255R1 mobility and accessibility parameters may reflect a tight fold in the peptide backbone at this point. It is also noteworthy that the proper folding of the epitope is dependent on the presence of phosphatidylethanolamine as a chaperone (*46*).

Importantly, each of the 20 Cys replacement mutants examined here displays normal transport activity (*15*). Therefore, it is likely that the mutants retain near native structure even with the attached spin-label. Although the nitroxide side chain must induce at least some perturbation in the backbone and the position of the side chain, it is unlikely that the effects are of sufficient magnitude to alter the overall interpretation of the data (*5*, *13*). It is also relevant that the permease is embedded in DM micelles in these studies rather than in a phospholipid bilayer. However, it should be emphasized that studies utilizing site-directed fluorescence (*47*, *48*), introduction of engineered metal binding sites (i.e. bis-His residues; *22*, *49*, *50*), and two monoclonal antibodies that bind to conformational epitopes (*27*, *51*) indicate that the permease retains near native structure in DM.

ACKNOWLEDGMENT

We are grateful for the excellent technical assistance provided by Leslie Wang.

REFERENCES

1. Kaback, H. R. (1996) in *Handbook of Biological Physics: Transport Processes in Eukaryotic and Prokaryotic Organisms* (Konings, W. N., Kaback, H. R., and Lolkema, J. S., Eds.) pp 203−227, Elsevier, Amsterdam.
2. Kaback, H. R., Voss, J., and Wu, J. (1997) *Curr. Opin. Struct. Biol. 7*, 537−542.
3. Kaback, H. R. (1997) *Proc. Natl. Acad. Sci. U.S.A. 94*, 5539−5543.
4. Hubbell, W. L., and Altenbach, C. (1994) *Curr. Opin. Struct. Biol. 4*, 566−573.
5. Hubbell, W. L., and Altenbach, C. A. (1994) in *Membrane Protein Structure* (White, S. H., Ed.) pp 224−248, Oxford University Press, New York.
6. Hubbell, W. L., Mchaourab, H. A., Altenbach, C., and Lietzow, M. A. (1996) *Structure 4*, 779−783.
7. Anthony-Cahill, S. J., Benfield, P. A., Fairman, R., Wasserman, Z. R., Brenner, S. L., Stafford, W. d., Altenbach, C., Hubbell, W. L., and DeGrado, W. F. (1992) *Science 255*, 979−983.
8. Rabenstein, M. S., and Shin, Y.-K. (1995) *Proc. Natl. Acad. Sci. U.S.A. 92*, 8239−8243.
9. Voss, J., Salwinski, L., Kaback, H. R., and Hubbell, W. L. (1995) *Proc. Natl. Acad. Sci. U.S.A. 92*, 12295−12299.
10. Voss, J., Hubbell, W. L., and Kaback, H. R. (1995) *Proc. Natl. Acad. Sci. U.S.A. 92*, 12300−12303.
11. Farrens, D. L., Altenbach, C., Yang, K., Hubbell, W. L., and Khorana, H. G. (1996) *Science 274*, 768−770.
12. Wu, J., Voss, J., Hubbell, W. L., and Kaback, H. R. (1996) *Proc. Natl. Acad. Sci. U.S.A. 93*, 10123−10127.
13. Mchaourab, H., Lietzow, M. A., Hideg, K., and Hubbell, W. L. (1996) *Biochemistry 35*, 7692−7704.
14. Voss, J., He, M., Hubbell, W., and Kaback, H. R. (1996) *Biochemistry 35*, 12915−12918.
15. Frillingos, S., Sahin-Tóth, M., Persson, B., and Kaback, H. R. (1994) *Biochemistry 33*, 8074−8081.
16. Ujwal, M. L., Jung, H., Bibi, E., Manoil, C., Altenbach, C., Hubbell, W. L., and Kaback, H. R. (1995) *Biochemistry 34*, 14909−14917.
17. King, S. C., Hansen, C. L., and Wilson, T. H. (1991) *Biochim. Biophys. Acta 1062*, 177−186.
18. Lee, J. L., Hwang, P. P., Hansen, C., and Wilson, T. H. (1992) *J. Biol. Chem. 267*, 20758−20764.
19. Sahin-Tóth, M., Dunten, R. L., Gonzalez, A., and Kaback, H. R. (1992) *Proc. Natl. Acad. Sci. U.S.A. 89*, 10547−10551.
20. Dunten, R. L., Sahin-Tóth, M., and Kaback, H. R. (1993) *Biochemistry 32*, 3139−3145.
21. Sahin-Tóth, M., and Kaback, H. R. (1993) *Biochemistry 32*, 10027−10035.
22. He, M. M., Voss, J., Hubbell, W. L., and Kaback, H. R. (1995) *Biochemistry 34*, 15661−15666.
23. Wu, J., Perrin, D., Sigman, D., and Kaback, H. (1995) *Proc. Natl. Acad. Sci. U.S.A. 92*, 9186−9190.
24. Frillingos, S., Wu, J., Venkatesan, P., and Kaback, H. R. (1997) *Biochemistry 36*, 6408−6414.
25. Carrasco, N., Tahara, S. M., Patel, L., Goldkorn, T., and Kaback, H. R. (1982) *Proc. Natl. Acad. Sci. U.S.A. 79*, 6894−6898.
26. Carrasco, N., Viitanen, P., Herzlinger, D., and Kaback, H. R. (1984) *Biochemistry 23*, 3681−3687.
27. Sun, J., Wu, J., Carrasco, N., and Kaback, H. R. (1996) *Biochemistry 35*, 990−998.
28. Sun, J., Frillingos, S., and Kaback, H. R. (1997) *Protein Sci. 6*, 1503−1510.
29. Wu, J., and Kaback, H. R. (1997) *J. Mol. Biol. 270*, 285−293.
30. Consler, T. G., Persson, B. L., Jung, H., Zen, K. H., Jung, K., Prive, G. G., Verner, G. E., and Kaback, H. R. (1993) *Proc. Natl. Acad. Sci. U.S.A. 90*, 6934−6938.
31. Froncisz, W., and Hyde, J. S. (1982) *J. Magn. Reson. 47*, 515−521.
32. Haldar, K., Olsiewski, P. J., Walsh, C., Kaczorowski, G. J., Bhaduri, A., and Kaback, H. R. (1982) *Biochemistry 21*, 4590−4596.
33. Hubbell, W. L., Froncisz, W., and Hyde, J. S. (1987) *Rev. Sci. Instrum. 58*, 1879−1886.
34. Altenbach, C., Flitsch, S. L., Khorana, H. G., and Hubbell, W. L. (1989) *Biochemistry 28*, 7806−7812.
35. Farahbakhsh, Z. T., Altenbach, C., and Hubbell, W. L. (1992) *Photochem. Photobiol. 56*, 1019−1033.
36. Altenbach, C., Yang, K., Farrens, D., Khorana, G. H., and Hubbell, W. L. (1996) *Biochemistry 35*, 12470−12478.
37. McKenna, E., Hardy, D., and Kaback, H. R. (1992) *Proc. Natl. Acad. Sci. U.S.A. 89*, 11954−11958.
38. Wu, J., and Kaback, H. R. (1996) *Proc. Natl. Acad. Sci. U.S.A. 93*, 14498−14502.
39. Greenhalgh, D. A., Altenbach, C., Hubbell, W. L., and Khorana, H. G. (1991) *Proc. Natl. Acad. Sci. U.S.A. 88*, 8626−8630.
40. Altenbach, C., Marti, T., Khorana, H. G., and Hubbell, W. L. (1990) *Science 248*, 1088−1092.
41. Foster, D. L., Boublik, M., and Kaback, H. R. (1983) *J. Biol. Chem. 258*, 31−34.
42. Zen, K. H., McKenna, E., Bibi, E., Hardy, D., and Kaback, H. R. (1994) *Biochemistry 33*, 8198−8206.
43. Resek, J. F., Farahbakhsh, Z. T., Hubbell, W. L., and Khorana, H. G. (1993) *Biochemistry 32*, 12025−12032.
44. Sun, J., and Kaback, H. R. (1997) *Biochemistry 36*, 11959−11965.
45. Pellequer, J. L., Westhof, E., and Van Regenmortel, M. H. (1993) *Immun. Lett. 36*, 83−99.
46. Bogdanov, M., Sun, J., Kaback, H. R., and Dowhan, W. (1996) *J. Biol. Chem. 271*, 11615−11618.
47. Jung, K., Jung, H., and Kaback, H. R. (1994) *Biochemistry 33*, 3980−3985.
48. Wu, J., Frillingos, S., Voss, J., and Kaback, H. R. (1994) *Protein Sci. 3*, 2294−2301.
49. Jung, K., Voss, J., He, M., Hubbell, W. L., and Kaback, H. R. (1995) *Biochemistry 34*, 6272−6277.
50. He, M. M., Voss, J., Hubbell, W. L., and Kaback, H. R. (1995) *Biochemistry 34*, 15667−15670.
51. Sun, J., Li, J., Carrasco, N., and Kaback, H. R. (1997) *Biochemistry 36*, 274−280.

BI971726J